



Science Arts & Métiers (SAM)

is an open access repository that collects the work of Arts et Métiers Institute of Technology researchers and makes it freely available over the web where possible.

This is an author-deposited version published in: <https://sam.ensam.eu>
Handle ID: <http://hdl.handle.net/10985/25381>



This document is available under CC BY license

To cite this version :

Jean-Patrick GOULMY, L. TOUALBI, V. BOYER, P. KANOUTE, D. RETRAINT, E. ROUHAUD - A model for the influence of work hardening and microstructure on the evolution of residual stresses under thermal loading – Application to Inconel 718 - European Journal of Mechanics - A/Solids - Vol. 107, p.105361 - 2024

Any correspondence concerning this service should be sent to the repository

Administrator : scienceouverte@ensam.eu





Full Length Article

A model for the influence of work hardening and microstructure on the evolution of residual stresses under thermal loading – Application to Inconel 718

J.P. Goulmy^{a,*}, L. Toualbi^b, V. Boyer^c, P. Kanoute^b, D. Reiraint^c, E. Rouhaud^d

^a Arts et Metiers Institute of Technology, MSMP, HESAM Université, F-13617, Aix-en-Provence, France

^b Onera - The French Aerospace Lab, Département Matériaux et Structures, F-92322, Châtillon, France

^c Laboratoire des Systèmes Mécaniques et d'Ingénierie Simultanée (LASMIS), Université de Technologie de Troyes (UTT), 10000, Troyes, France

^d GAMMA3 Université de Technologie de Troyes (UTT), 10000, Troyes, France

ARTICLE INFO

Keywords:

Inconel 718
Shot peening
Residual stresses
Work hardening
Thermal relaxation

ABSTRACT

This study proposes a model for the influence of work hardening and microstructure on the thermal relaxation of residual stresses. To construct such a model, an experimental campaign is first conducted on shot peened samples of Inconel 718 to generate different levels of residual stress and work hardening. The effect of the grain size and the size of the strengthening precipitates is investigated by producing two modified microstructures. Two shot peening conditions are used to introduce several profiles of residual stress and work hardening. These profiles are evaluated using X-ray diffraction. A thermal loading is then applied at 550 °C with varying holding times, leading to a rapid but not complete relaxation of the residual stresses and work hardening. The experimental results exhibit the fact that the work hardening levels have a significant influence on this relaxation while the grain size and the size of the strengthening precipitates have a very moderate influence. Based on these experimental results, a model is proposed that considers the influence of work hardening on the thermal relaxation of residual stresses with some predictive applications. It is therefore possible to estimate the relaxation of residual stresses at any point on a shot peened part.

1. Introduction

In order to improve the fatigue life of critical components, surface improvement methods such as shot peening are widely used in the aerospace industry. This process generates superficial compressive residual stresses that tend to delay fatigue crack initiation and prevent small crack propagation (Benedetti et al., 2010), (Bhuiyan et al., 2012), (Gerin et al., 2017), (Klotz et al., 2018), (Qin et al., 2022). For structures that experience high temperature variations in service, these surface enhancement methods are only efficient if the thermo-mechanical relaxation of the generated residual stress field is moderate at operating temperatures. It is however observed that relaxation due to thermal effects is far from being negligible in high-temperature fatigue tests (Prevéy, 2000). It is therefore important to understand the mechanisms that induce the thermal relaxation of residual stresses in order to further input these effects into a model. One of the critical points is to estimate the kinematic and time constants of this relaxation.

The nickel-based superalloy Inconel 718 is widely used in the aeronautical industry. In its standard metallurgical state known as Direct Aged (DA), this alloy features a microstructure with a γ matrix composed of grains of about 5 μm , γ'/γ'' strengthening precipitates of a few nanometers, a δ phase anchored at the grain boundaries, as well as carbides and nitrides that locally harden the matrix (Pieraggi and Uginet, 1994), (Chen and Chaturvedi, 1997), (Schafrik et al., 2001), (Alexandre et al., 2004). Subjected to temperatures close to 550 °C, Inconel 718 turbine discs undergo thermo-mechanical stresses in service. These discs can present microstructural heterogeneities because of their manufacturing process history; they can also undergo more than ten conditions of shot peening treatment, depending on their geometry. The in-service evolution of residual stresses in these parts can therefore be particularly diverse and complex. In order to evaluate the benefits of shot peening on the fatigue life of these parts, it is necessary to understand the microstructural changes induced by shot peening and their influence on the thermal relaxation of residual stresses. Inconel 718 thus

* Corresponding author.

E-mail address: jean-patrick.goulmy@ensam.eu (J.P. Goulmy).

Table 1

Composition of the Inconel 718 DA alloy (Wt%).

Ni	Fe	Cr	Mo	Al	Ti	Nb	Si	C
54.18	17.31	17.97	2.97	0.56	1	5.39	0.1	0.023

Table 2

Shot peening conditions applied to the different microstructures.

Name	Shot	Almen Intensity	Coverage
SP1	S110 steel	12–13A	125%
SP2	S110 steel	22–23A	200%

constitutes a material of interest to study and model residual stress relaxation due to thermal loading.

Clearly, microstructural parameters of Inconel 718 have a significant influence on the tensile, fatigue, and creep properties (Pieraggi and Uginet, 1994), (Chen and Chaturvedi, 1997), (Schafrik et al., 2001). Furthermore, previous studies (Goulmy et al., 2021a), (Goulmy et al., 2021b) have highlighted the influence of microstructural modifications on the residual stress and work hardening profiles induced by shot peening. It was shown that work hardening is significantly affected by a change in grain size. On the contrary, changing the grain size or the size of the strengthening precipitates γ'/γ'' appears to have minimal effect on the residual stress profile. It is then useful to define how these different profiles relax with time.

Many authors (Surface Integrity, 1989), (Masmoudi Khebou, 1990), (Lillamand, 1999), (Hoffmeister et al., 2008), (Prevéy, 1987) have described the thermal relaxation of residual stresses caused by shot peening. By relaxation, it is here meant a lowering of the local absolute value of the residual stress level. The main observations are: (i) the higher the temperature, the higher the relaxation of the residual stresses combined with the fact that relaxation is negligible below a threshold temperature, except at the surface where a change may occur depending on the shot peening condition used; (ii) relaxation is observed at each depth of the profile, hence, the general shape of the profiles (position of the maximum stress, position of the tensile transition) is not changed, except above a certain temperature where a shift from the top of the profile to the core of the part is observed (iii) for a given temperature, the main evolution of the residual stresses takes place during the first instants of temperature holding, then, the residual stress profiles tend to asymptotic profiles with time.

The impact of work hardening on the relaxation of residual stresses has also previously been characterized in the literature (Prevéy, 2000), (Schulze et al., 1993), (Cammatt et al., 2005), (Juijerm and Altenberger, 2006), (Zhou et al., 2011), (Foss et al., 2013). Prévéy observed that there is a threshold value (3% of work hardening) below which no relaxation of residual stresses is observed (Prevéy, 2000). Above this threshold, many authors have shown that the greater the work hardening induced by shot peening, the greater the relaxation of residual stress (Prevéy, 2000), (Schulze et al., 1993), (Cammatt et al., 2005), (Zhou et al., 2011), (Foss et al., 2013). These studies explain that residual stress relaxation is related to the density of dislocations in the material: the higher the number of dislocations, the more the residual stresses relax. It is in particular observed that the laser shock process, known to induce low work hardening levels, results in much lower residual stress relaxation than shot peening (Prevéy, 2000). Prévéy also established that residual stress relaxation is influenced by the level of work hardening and not the method of work hardening introduction.

The residual stress and work hardening profiles resulting from the different manufacturing processes used for industrial parts vary considerably. Consequently, controlling the relaxation of residual stresses has become challenging and requires the development of appropriate models. The most widely used model for the thermal relaxation of residual stresses is the Zener-Wert-Avrami model

(Hoffmeister et al., 2008), (Juijerm and Altenberger, 2006), (Vöhringer and NIKU-LARI, 1987), (Berger and Gregory, 1999), (Feng et al., 2009). It predicts stress relaxation without taking work hardening into account. Its parameters are therefore only identified for a specific operating point (a microstructure, a position in a sample, a manufacturing process, and a temperature). Hoffmeister et al. proposed a more complex model to account for microstructural effects (Hoffmeister et al., 2008). Here again, the model depends on a specific operating point and is not able to predict the relaxation of residual stresses in depth unless a large set of measurements is available to identify a set of parameters for each test condition. Thus, although the influence of work hardening on the relaxation of residual stresses has been clearly established through several experimental observations, to date, there is no model available in the literature taking these effects into account. It should also be noted that the influence of the microstructure and its relationship to the effect of work hardening is relatively rarely, if ever, discussed in the literature.

The purpose of this paper is to investigate the impact of work hardening and microstructure on the thermal relaxation of residual stresses caused by shot peening on Inconel 718. The main objective is to propose a model that accurately accounts for these effects. This paper is composed of three sections. The first section describes the experimental methods starting with the description of the reference material microstructure of Inconel 718. In addition, this section presents the different thermal treatments proposed to obtain two complementary microstructures, as well as shot peening conditions and procedures to characterize residual stresses and work hardening. The second section presents and compares the results obtained after shot peening and after thermal relaxation at 550 °C of shot peened parts. The influence of work hardening and microstructure on the relaxation of residual stresses is discussed. The final section describes the proposed model for thermal relaxation of residual stresses accounting for the influence of work hardening. The developed analytical model is validated on a large set of data using complementary results from the literature.

2. Materials and methods

2.1. Inconel 718

The investigated material is Inconel 718 with a γ matrix; its composition is given in Table 1. The influence of the microstructure is evaluated through the study of three different microstructures. First, the *reference* microstructure, obtained after manufacturing and corresponding to the “as-received” material, known as Direct Aged (DA). The other two microstructures, namely coarse grain microstructure (CG) and coarse grain and coarse strengthening precipitates microstructure (CGCP), exhibit parameters that have been modified by means of a specific heat treatment history. The microstructure of CG was achieved by annealing at 1040 °C for 30 min, followed by δ phase precipitation treatment at 955 °C for 1 h, and finally by conventional γ'/γ'' strengthening precipitation treatment (8 h at 720 °C followed by cooling at 50 °C/h and aging at 620 °C for 8 h). The CGCP microstructure is characterized by coarse grains and large strengthening precipitates. The heat treatment sequence applied to the CG microstructure was also used, except for the final precipitation treatment of the γ' and γ'' phases. To increase the size of the precipitates, an overaging process was applied at 750 °C for 50 h. Please note that throughout the rest of this article, a color code has been used to refer to the three microstructures: the DA microstructure is referenced in blue, the CG microstructure in red and CGCP microstructure in orange.

2.2. Shot peening conditions

The shot peened samples are parallelepipeds of 20 × 15 × 10 mm in size. The samples underwent mechanical polishing to achieve a mirror finish before shot peening. The aim was to reduce residual stresses and work hardening caused by machining. XRD measurements were

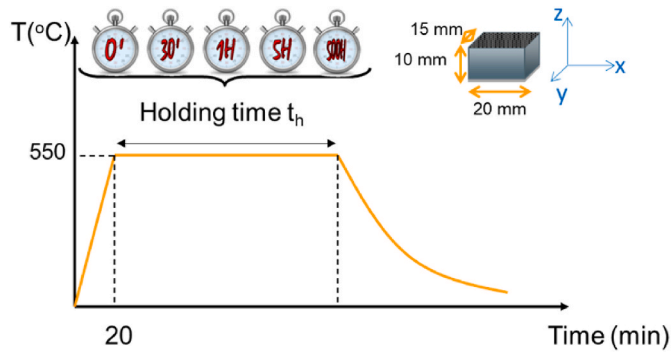


Fig. 1. Diagram of the thermal loading cycle applied to the samples with the definition of the holding time.

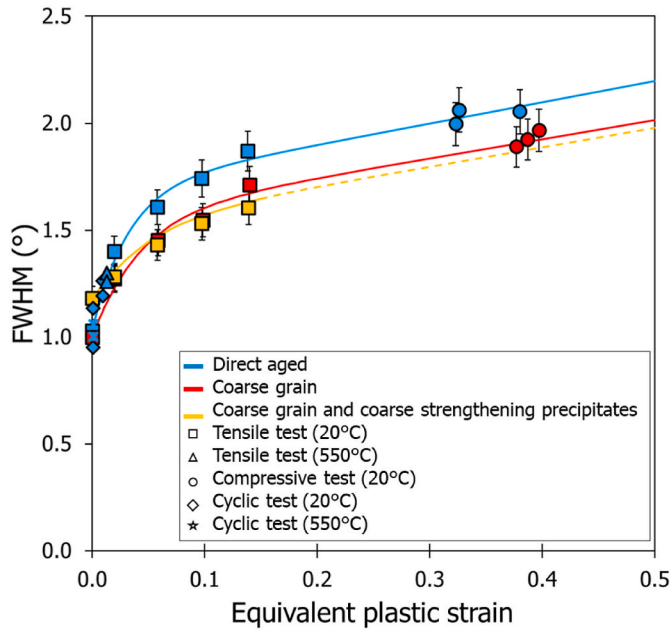


Fig. 2. The full width at half maximum (FWHM) as a function of equivalent plastic strain for different load histories, temperatures, and microstructures with corresponding calibration curves. (Goulmy et al., 2021a).

Table 3

The constants' values obtained for calibrating the full width at half maximum (FWHM) for the three microstructures, as defined by Eq. (1). (Goulmy et al., 2021a). Note that all constants are estimated to the nearest 0.01.

	Direct Aged (DA)	Coarse grain (CG)	Coarse grain and coarse precipitates (CGCP)
A_{FWHM}	0.66	0.56	0.35
B_{FWHM}	31.12	23.92	20.00
C_{FWHM}	0.99	0.90	0.90
D_{FWHM}	1.04	1.00	1.18

conducted to confirm the absence of residual stress (see Section 2.2). The samples underwent shot peening on one of their largest surfaces using a conventional nozzle and S110 steel shot. Two shot peening conditions (SP1 and SP2) were defined according to AFNOR standard NFL 06–832 (Norme AFNOR NFL 06, 1990). The shot peening parameters (see Table 2) were chosen for two reasons: (i) they are commonly applied to industrial components and (ii) they induce very different residual stress and work hardening gradients, which is necessary to validate the proposed methodology. The shot peening conditions were adjusted to take account for the fact that the change in grain size results in a reduction in

the strength of the modified microstructures. As a consequence, the conditions shown in Table 2 were chosen so that the coverage was identical for all three microstructures.

2.3. Thermal loading conditions

After shot peening, the samples were placed in a vacuum furnace and subjected to a temperature cycle without any mechanical loading; Fig. 1 illustrates the corresponding cycle. The rise in temperature lasts 20 min; the temperature is then maintained at 550 °C during a time lapse t_h called the “holding time” in the present article. Five different holding times were applied in this experimental campaign, ranging from 0 to 500 h. The samples were then placed in an argon stream for rapid cooling. Note that $t_h = 0$ corresponds to a sample that has undergone an increase and a decrease in temperature without any holding time.

2.4. Material characterization

2.4.1. Scanning Electron Microscope observations

The microstructural observations were conducted using a MERLIN Scanning Electron Microscope (SEM) with an accelerating voltage of 5 kV and a nominal current of 40 nA. To reveal the microstructure, including the strengthening precipitates γ' and γ'' , an ion polishing system was used to obtain a mirror-polished surface. The grain size was quantified using the Electron Backscattered Diffraction (EBSD) method. The data was acquired using a NORDIF CD camera operating at 30 fps coupled to a MERLIN SEM operating at 20 kV acceleration voltage and 40 nA nominal current.

2.4.2. X-ray diffraction measurements

X-ray diffraction measurements were conducted on the 311-diffraction peak at a 2θ angle of approximately 111° using a Seifert PTS diffractometer. The radiation source was a Co-K α tube with a wavelength of 1.79 Å, an accelerating voltage of 20 kV, and a nominal current of 4 mA. The sample preparation was identical to that used for microstructure characterization, as described above. Under these conditions, the X-ray penetration depth was estimated to be between 2 and 4 μm , and the analyzed surface was a few millimeters wide. The X-ray data were processed using classical methods (Lu, 1996), specifically the $\sin^2\psi$ method with analysis of eleven ψ angles to determine the depth profiles. Line broadening was used as a measure for work hardening (see Section 1.4.3 for more details). This was defined by the full width at half maximum (FWHM) of the peaks obtained by a Voigt pseudo-profile fit. For in-depth evaluation of the quantities of interest, electrolytic polishing with an average step of 40 μm was carried out. A correction method was applied which showed that the material removal had a negligible effect on the residual stress values. Residual stresses and peak widths were measured in two directions, but no significant differences were found. This confirms that shot peening induces an in-plane equibiaxial stress state. The FWHM depth profile was evaluated before shot peening, and a consistent FWHM value was observed for all untreated samples, as shown by the triangular data points in Fig. 5. After shot peening, three residual stress and FWHM profiles were determined at different locations on the surface of the samples for each microstructure to study the dispersion of these parameters. Following heat treatment, one residual stress and FWHM profile was measured for each microstructure.

2.4.3. Procedure of work hardening characterization

If the method for evaluating the residual stress values from X-Ray diffraction measurements is well established, the evaluation of the work hardening requires the implementation of a calibration method (Prevéy, 1987), (Foss et al., 2013), (Kamaya et al., 2004), (Hoffmeister et al., 2011), (Soady et al., 2013). This method has been successfully applied to the microstructures studied in this paper (Goulmy et al., 2021a), (Goulmy et al., 2021b) and has demonstrated its interest in validating

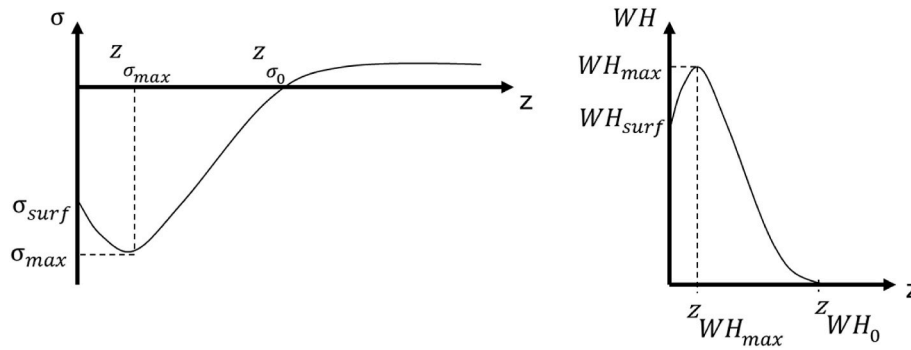


Fig. 3. Syntax used to describe the profiles of residual stress and work hardening induced by shot peening induced.

Table 4

X-ray diffraction measurement matrix. p: profile with measurements up to at least 300 μm depth for residual stresses and work hardening; pp: partial profile, up to 150 μm.

Holding time t_h (h)	Microstructure								
	Direct Aged (DA)			Coarse grain (CG)			Coarse grain and coarse precipitates (CGCP)		
	Unshot	SP1	SP2	Unshot	SP1	SP2	Unshot	SP1	SP2
Untreated	3 p	3 p	3 p	3 p	3 p	3 p	3 p	3 p	3 p
0	–	1 p	1 p	–	1 p	1 p	–	1 p	1 p
0.5	–	1 p	1 p	–	1 p	1 p	–	1 p	1 p
1	–	1 p	1 p	–	1 p	1 p	–	1 p	1 p
5	–	1 p	1 p	–	1 p	1 p	–	1 p	1 p
50	–	1 p	1 p	–	1 p	1 p	–	1 p	1 p
500	–	1 pp	1 p	–	1 pp	1 pp	–	1 pp	1 pp

the modeling of the shot peening process (Goulmy et al., 2023). Work hardening is identified with the equivalent plastic strain noted ϵ_p as discussed in (Goulmy et al., 2021a). The relationship between the FWHM obtained by X-ray diffraction and the work hardening is presented in Fig. 2 for the three Inconel 718 microstructures and is modeled by (Prevéy, 1987):

$$FWHM(\epsilon_p) = A_{FWHM} (1 - e^{-B_{FWHM}\epsilon_p}) + C_{FWHM} \epsilon_p + D_{FWHM} \quad \text{Eq. 1}$$

The parameters that have been evaluated are A_{FWHM} , B_{FWHM} , C_{FWHM} and D_{FWHM} (Goulmy et al., 2021a). They are given in Table 3. The work hardening induced by shot peening can be determined by inverting Eq. (1). A typical work hardening profile obtained by this method is shown in Fig. 3.

The parameters for the work hardening characterization were identified for each microstructure; this method can be used only if no microstructural modification is observed during any of the treatments (thermal or mechanical) that the samples undergo (Goulmy et al., 2021a), (Goulmy et al., 2021b). Scanning electron microscope analyses were therefore performed after shot peening and after the thermal treatment to assess the evolution of the microstructure.

2.4.4. Experimental plan

To conclude this Materials and Methods Section, the complete X-ray diffraction measurement plan is presented in Table 4. For each condition and each microstructure, the number of profiles acquired in depth is indicated. Fig. 3 also presents the syntax used to describe the shape of the shot peen induced residual stress and work hardening profiles.

3. Experimental results

3.1. Microstructural observations

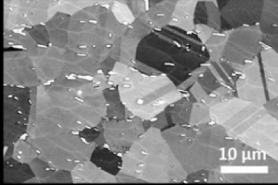
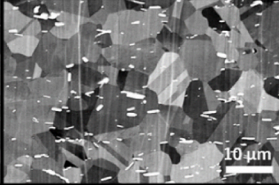
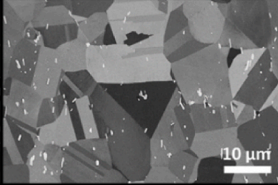
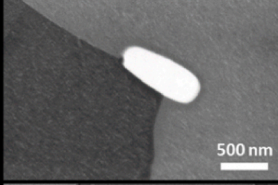
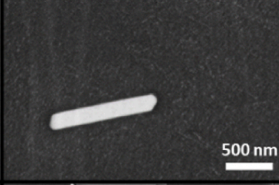
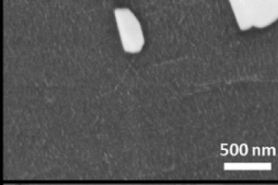
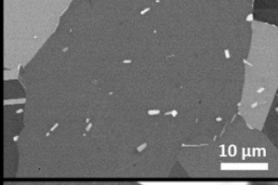
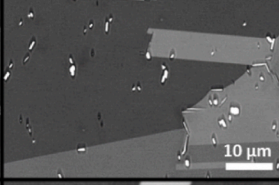
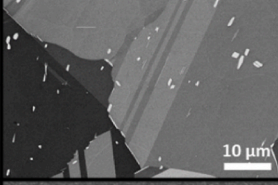
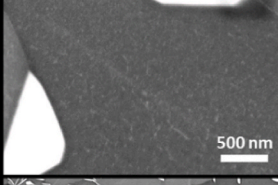
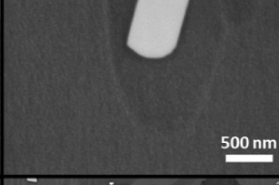
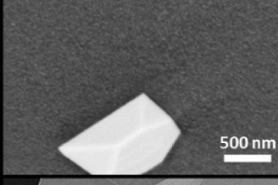
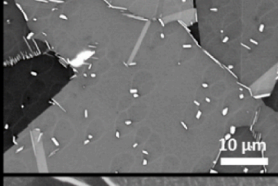
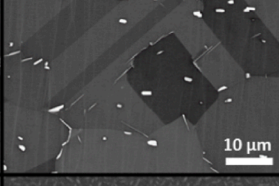
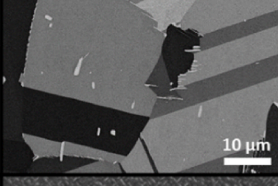
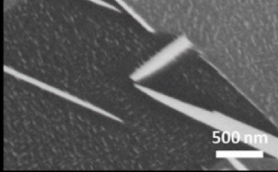
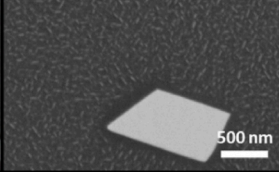
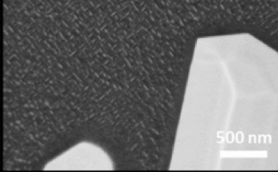
To detect any microstructural evolution, SEM observations were carried out on the three investigated microstructures before shot

peening, after shot peening alone, and after shot peening followed by a holding time of 500 h at 550 °C. The results of these observations are presented in Table 5. Only the results with the higher shot peening condition (SP2) are detailed here, as similar results were obtained for the SP1 shot peening condition. Table 6 summarizes the microstructural characterizations obtained from SEM observations and EBSD analyses before shot peening. An average grain size of about 5 μm is observed for the DA microstructure, while the other two microstructures have average grain sizes around 35 μm. The size of the strengthening precipitates is similar for the DA and CG microstructures (10–20 nm), but much larger for the CGCS microstructure with a size of 100–200 nm. Binarization of the SEM images was performed to assess the morphology and distribution of the δ phase. A form factor of 0.9 was arbitrarily chosen to differentiate needle-shaped from globular precipitates. The proportion of the δ phase in the CG and CGCP microstructures is between 1.4% and 1.7%, values that remain in the same order of magnitude as for the DA microstructure (2.3%). The proportion of needles and globules (40% and 60%, respectively) is also similar for the three microstructures. Comparing the DA microstructure with the CG microstructure thus gives access to the effect of grain size. Similarly, the comparison of the CG and the CGCP microstructures allows studying the influence of the size of the strengthening precipitates.

The SEM characterization of a sample shot peened under SP2 conditions, the most severe, shows a great stability of the microstructure (Fig. 4). It confirms that the shot peening conditions applied in this work do not induce any change in grain size or orientation, or in the size of the strengthening precipitates. Similarly, the SEM characterization performed after the thermal loadings at 550 °C revealed no microstructural change in terms of grain size or strengthening precipitate size, showing morphologically stable microstructures over time (Table 5). The temperature of 550 °C used in this study for the thermal loading does not induce any microstructural change in the strengthening precipitates, even in the presence of work hardening at the material surface. It should be noted that an increase in the rate of γ'' precipitates was observed in a previous study for shot peened samples subjected to aging treatments at

Table 5

SEM microstructural characterizations carried out on the different microstructures: before shot peening, after shot peening (SP2) and after shot peening (SP2) and 500 h at 550 °C. The results obtained for the SP1 shot peening condition are similar.

		Before shot peening	After shot peening SP2 (Close to the surface)	After shot peening SP2 and 500h at 550°C (Close to the surface)
DA microstructure	Grains			
	Strengthening precipitates			
CG microstructure	Grains			
	Strengthening precipitates			
CGCP microstructure	Grains			
	Strengthening precipitates			

700 °C (Cai et al., 2006); this can be explained by the higher temperature of the treatment. These analyses validate that, since no microstructural change is observed, the calibration curves shown in Fig. 2 can be used to evaluate the work hardening gradient introduced by shot peening, before and after the thermal loading.

3.2. Residual stresses and work hardening after shot peening

The residual stress and work hardening profiles determined by X-ray diffraction for the three microstructures before shot peening and after SP1 and SP2 conditions are now compared (Fig. 5). The dashed lines correspond to a fit obtained for each microstructure and each shot peening condition. Despite the fluctuations from one sample to another,

clear trends are obtained between the two investigated shot peening conditions.

The work hardening is clearly affected by the shot peening conditions, both in terms of value and depth. For example, for the DA microstructure, the average surface value is changed by almost 50% between the SP1 and SP2 conditions ($WH_{surf} = 20\%$ and $WH_{surf} = 40\%$ respectively). An increase in shot peening coverage and intensity results in a higher maximum compressive residual stress σ_{max} . The associated depth is also affected ($z_{\sigma_{max},SP1} = 50 \mu\text{m}$; $z_{\sigma_{max},SP2} = 80 \mu\text{m}$), as the size of the compression zone ($z_{\sigma_0,SP1} = 175 \mu\text{m}$; $z_{\sigma_0,SP2} = 225 \mu\text{m}$). At the surface, the residual stress values are relatively similar ($\sigma_{surf,SP1} \approx \sigma_{surf,SP2} \approx -700 \text{ MPa}$). Similar trends are observed for both CG and CGCP microstructures.

Table 6

For the three investigated microstructures: mean size of the grain and of the strengthening precipitates, and δ phase characteristics.

	Direct Aged microstructure	Coarse grain microstructure	Coarse strengthening precipitates microstructure
Average grain size (μm)	4.2	34.7	36.8
Strengthening precipitates size (nm)	$\sim 10 - 20$	$\sim 10 - 20$	$\sim 100 - 200$
δ phase area fraction	2.3%	1.4%	1.7%
δ phase morphology	$43 \pm 2\%$ needles	$36 \pm 2\%$ needles	$41 \pm 2\%$ needles
	$57 \pm 2\%$ globules	$64 \pm 2\%$ globules	$59 \pm 2\%$ globules

The residual stress differences remain below 100 MPa along the profiles when comparing the three microstructures. Thus, changing the grain size or the strengthening precipitates size has little impact on the residual stresses. However, the work hardening is strongly affected by the microstructural modifications. An increase in grain size implies an increase in surface work hardening of more than 25% for both investigated shot peening conditions. However, the thickness of the work hardened area is only slightly altered.

These results highlight the influence of both the shot peening conditions and the microstructure on the residual stress and work hardening profiles.

Table 7 presents the minimum and maximum values encountered for each condition for the DA microstructure (see notations in Fig. 3) with the purpose of characterizing experimental dispersion. This experimental dispersion may come from: measurement errors, microstructural variation from one sample to another, or the non-repeatability of the

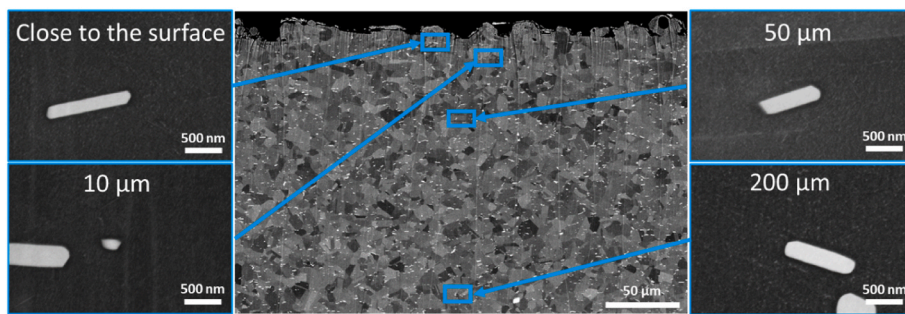


Fig. 4. SEM images at different depth for DA microstructure after SP2 shot peening.

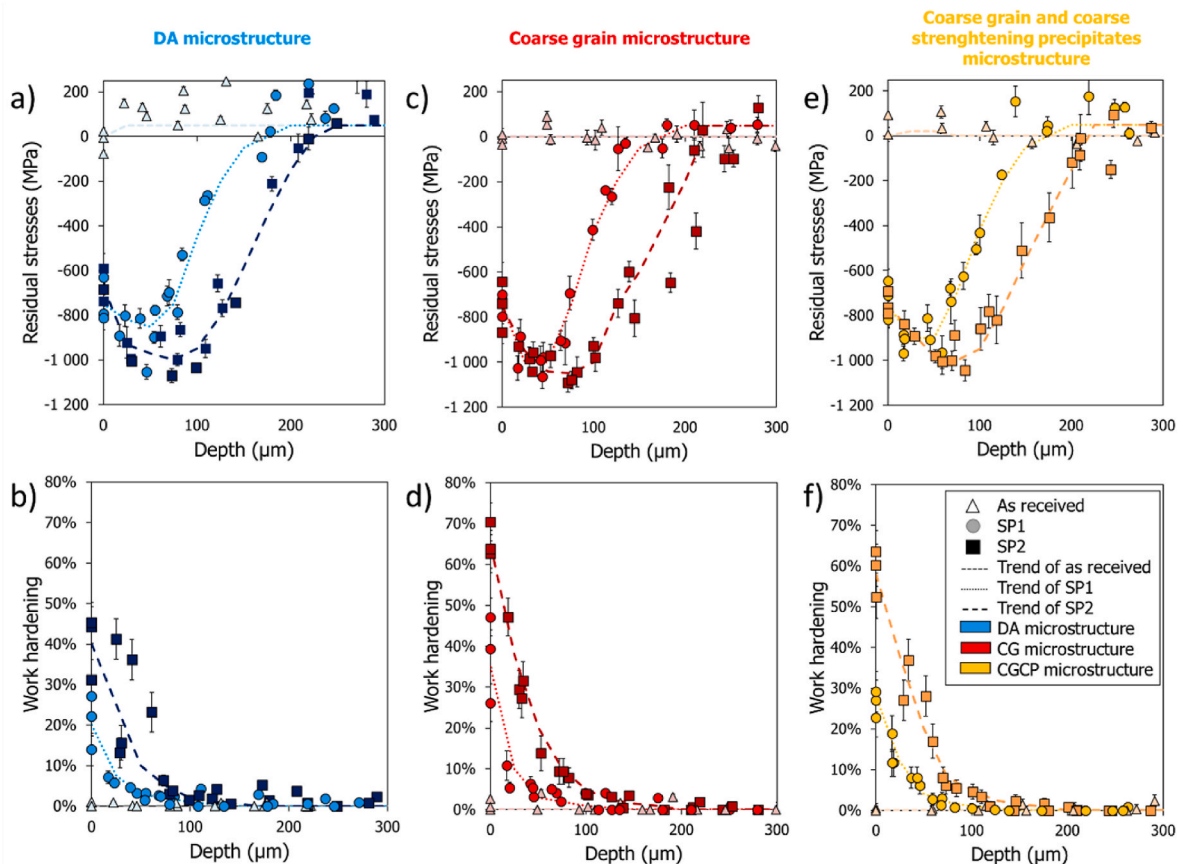


Fig. 5. Residual stress and work hardening profiles determined by X-ray diffraction on the three microstructures prior and after SP1, SP2 peening conditions.

Table 7

Summary of variations encountered for the two SP1 and SP2 shot peening conditions for the DA microstructure.

	SP1		SP2	
	Min	Max	Min	Max
σ_{surf} (MPa)	-600	-800	-600	-850
σ_{max} (MPa)	-800	-1050	-900	-1150
$z_{\sigma_{max}}$ (μm)	40	60	70	90
z_{σ_0} (μm)	120	200	200	250
WH_{max} (%)	15	30	20	45
WH_{surf} (%)	15	30	20	45
$z_{WH_{max}}$ (μm)	0	0	0	0
z_{WH_0} (μm)	75	170	100	200

shot peening process. These three possible sources of dispersion have been investigated and characterized. They are described in detail below.

- The measurement conditions are the same for all the samples, so the error is evaluated for all measurements around 20 MPa. Therefore, the observed variations cannot be specifically due to this aspect.
- Concerning the influence of the microstructure, the analyses in terms of grain size, distribution, and size of strengthening precipitates or crystalline orientation do not show any notable difference between the different samples. Looking at the DA microstructure compared to the two modified microstructures, the small differences in terms of the average value of the measured residual stresses or work hardening (Fig. 5) show that the microstructural variations, even of significant, can be neglected in front of the experimental variability related to the shot peening itself.

- Indeed, it is classical observed that the shot peening process shows a wide scatter of experimental residual stress results (Vöhringer and NIKU-LARI, 1987). This dispersion is generally related to an inherent variability of many parameters related to the shot stream, such as size, shape, hardness, impact angle and shot peening time. One way to account for this dispersion is to use the Monte Carlo simulation technique by introducing variability in the process parameters to predict the residual stress field (Fathallah et al., 1998), (Atig et al., 2018). The influence of the shot peening process on the repeatability of the measurements appears to be the most detrimental aspect of the experimental dispersion. Since it is difficult to control, a repetition of the measurements on different samples is often recommended to obtain a better accuracy. Experimental standard deviations of the order of 100 MPa for the residual stresses and of the order of 10% for the work hardening were obtained at the surface for all the microstructures. The standard deviation seems to decrease with depth.

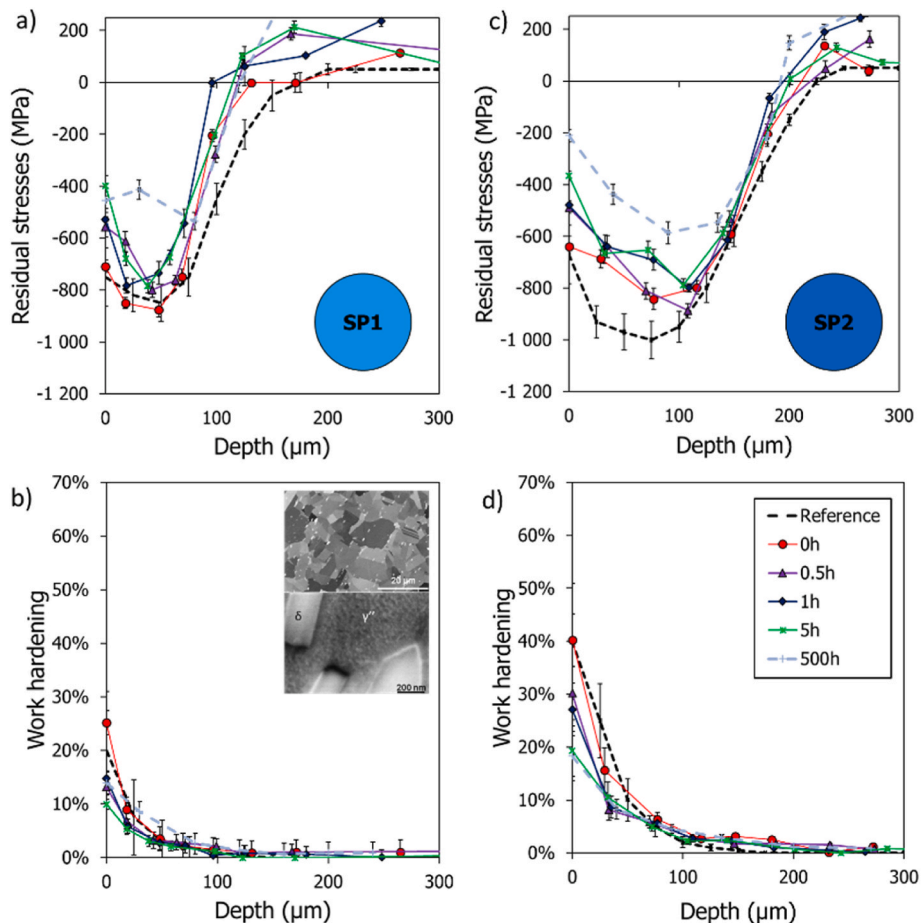


Fig. 6. Residual stress and work hardening profiles, for different holding times at 550 °C, for Inconel 718 DA microstructure, SP1 and SP2 conditions.

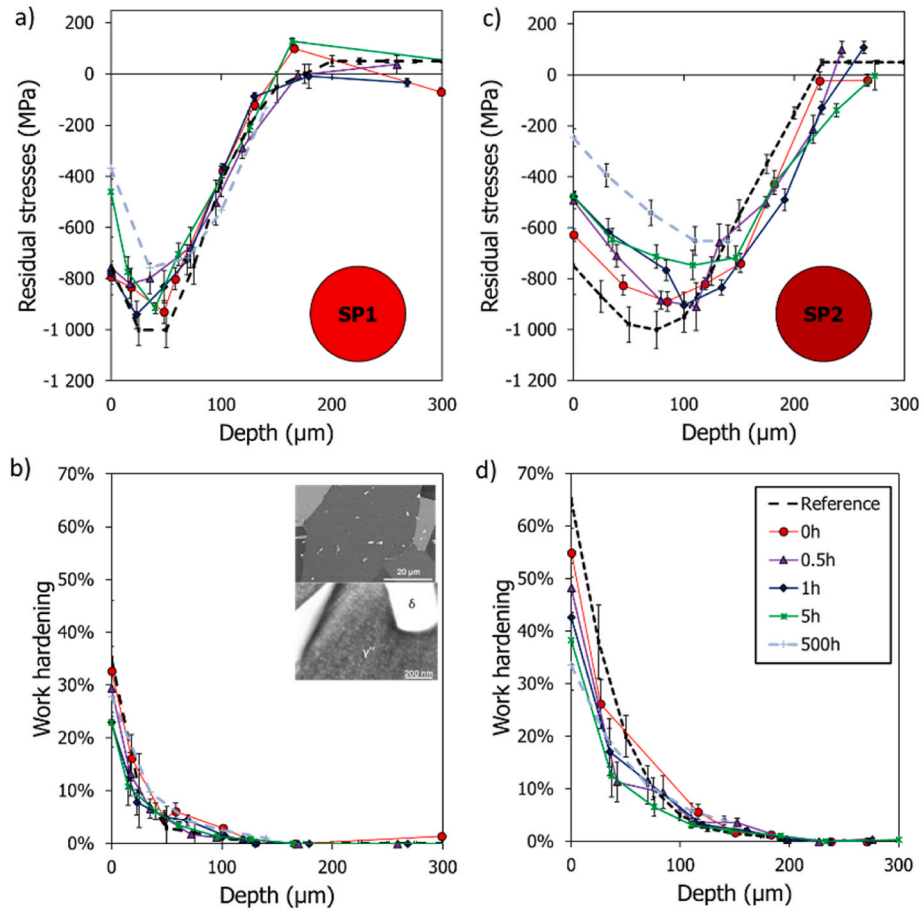


Fig. 7. Residual stress and work hardening profiles for different holding times at 550 °C, for Inconel 718 coarse grain microstructure, SP1 and SP2 conditions.

These results are consistent with those obtained by Daoud et al. in the simulation of the shot peening process (Daoud et al., 2021).

3.3. Residual stresses and work hardening after a thermal loading

The residual stresses and work hardening determined after thermal loading are now being studied. The first part is devoted to the study of the profiles. The second part focuses on the evolution of the key parameters identified in Fig. 3, which will serve as the basis for a model to estimate the relaxation of residual stresses.

3.3.1. Residual stress and work hardening profiles after thermal loading

The residual stress and work hardening profiles were analyzed to track their evolution after the shot peened samples were subjected to different holding times at 550 °C. As the relaxation under thermal loading is isotropic, only the component in the \vec{x} direction of the stress was studied (see caption of Fig. 1). Note that a distinction is made between samples that have not undergone thermal loading and those that have undergone a temperature rise and fall ($t_h = 0$). Except for a few measured points related to the SP2 shot peening condition, the difference is small between the reference and the samples that have undergone a holding time $t_h = 0$: the rise and fall in temperature do not trigger any relaxation.

Fig. 6 shows the residual stress and work hardening profiles obtained after thermal loading for the DA microstructure, shot peened under SP1 (Fig. 6a and b.) and SP2 (Fig. 6c and d.) conditions. Both shot peening conditions present the same evolution of the profiles. The residual stresses and work hardening induced by shot peening are only partially relaxed during thermal loading, even for the longest holding times. The

depth associated with the maximum value of compressive residual stresses $z_{\sigma_{max}}$ is not affected by the duration of the thermal holding at 550 °C. On the contrary, for the SP1 condition, the depth at which the residual stresses become positive z_{σ_0} undergoes a slight decrease with a holding time at 550 °C, which is not observed for the SP2 conditions. It is interesting to note that the surface residual stress that corresponds to the most intense level of work hardening, experiences the greatest relaxation. This relaxation is even more pronounced for the SP2 condition: at the surface where the work hardening value is about 40%, the compressive residual stress value evolves from -600 MPa to -200 MPa.

Figs. 7 and 8 show the residual stress and work hardening profiles for the CG and CGCP microstructures, respectively. It is noteworthy for these modified microstructures that even at very high levels of surface work hardening (over 60% for the CG and CGCP microstructures under SP2 conditions), the relaxation of residual stresses is only partial after several hundred hours at 550 °C. Again, the depth associated with the maximum value of compressive residual stresses $z_{\sigma_{max}}$ and that at which the residual stresses are positive z_{σ_0} appear to be relatively unaffected by the increase holding time. Similar to what was observed in the DA microstructure, the higher the level of work hardening, the higher the relaxation of residual stresses. The highest levels of relaxation are then found at the surface.

The main information to be drawn from these results is that the effects of shot peening, although partially reduced, are still present even after being exposed to a purely thermal loading at 550 °C for several hundred hours. It is therefore of particular interest to be able to model the residual stress relaxation at any point on the part, in order to know the residual stress profile at any point in time.

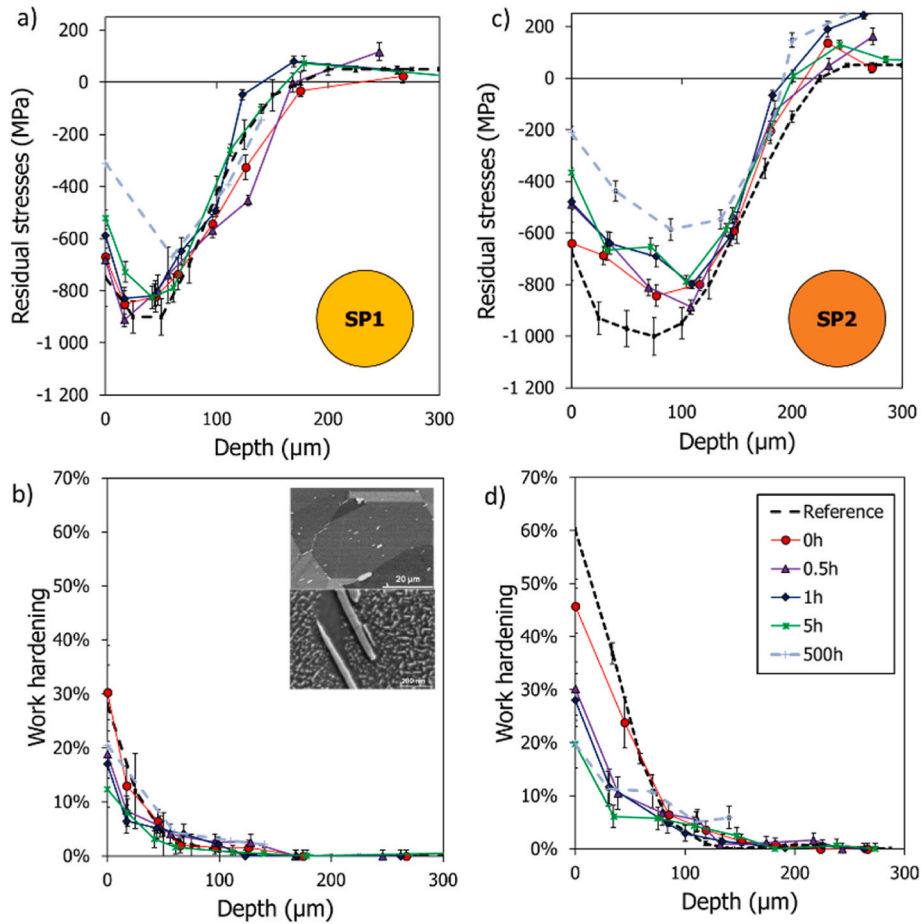


Fig. 8. Residual stress and work hardening profiles for different holding times at 550 °C, for Inconel 718 coarse grain and coarse strengthening microstructure, SP1 and SP2 conditions.

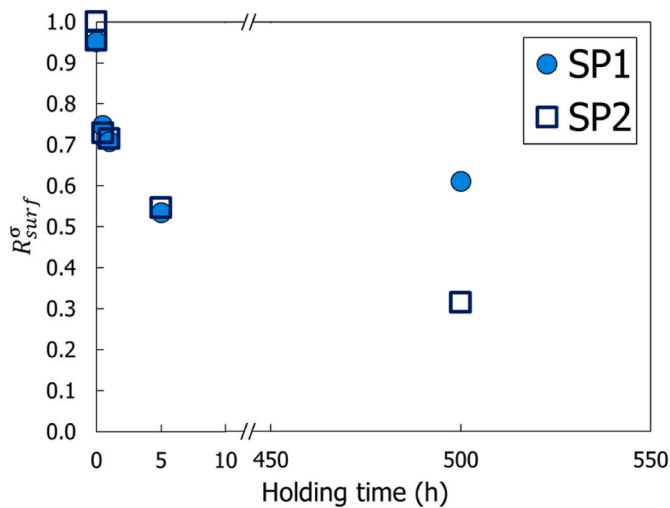


Fig. 9. Evolution of R_{surf}^{σ} as a function of time at 550 °C for the DA microstructure and the two SP1 and SP2 shot peening conditions; note the change in scale for the smaller holding time axis.

3.3.2. Definition of ratios to quantify relaxation

Ratios are here defined to quantify the relaxation of the residual stresses and the work hardening due to thermal loading. We first define reference profiles corresponding to the profiles determined after shot peening, for which, by definition, there is no relaxation. These reference

profiles are respectively noted, $\sigma_{ref}(z)$ for the residual stresses and $WH_{ref}(z)$ for work hardening. The experimental reference profiles are all presented in Fig. 5 as a function of the depth z for different microstructures and shot peening conditions.

Several profiles of residual stress and work hardening were evaluated after thermal loading for different holding times t_h (see Fig. 1 for the definition of t_h). These profiles are noted $\sigma(t_h, z)$ for the residual stresses and $WH(t_h, z)$ for work hardening, respectively, and are presented in Figs. 6–8 as a function of the depth z for different microstructures and shot peening conditions.

To quantify the relaxation, we define the ratios $R^{\sigma}(t_h, z)$ for residual stresses and $R^{WH}(t_h, z)$ for work hardening such that:

$$R^{\sigma}(t_h, z) = \frac{\sigma(t_h, z)}{\sigma_{ref}(z)} \quad \text{and} \quad R^{WH}(t_h, z) = \frac{WH(t_h, z)}{WH_{ref}(z)} \quad \text{Eq. 2}$$

Thus, when the ratios are equal to 1, no relaxation is observed; if the ratios were equal to 0, all the residual stresses or work hardening would have vanished.

3.3.3. Evolution of the surface and maximum values of residual stresses and work hardening with thermal loading

To simplify the analysis, representative points have been identified on the profiles of the residual stress and work hardening shown in Figs. 6–8. The evolution of these specific values is here studied as a function of the holding time t_h . For residual stress, the surface residual stress σ_{surf} and the maximum value σ_{max} at depth $z_{\sigma_{max}}$ were considered. For work hardening, the value at the surface WH_{surf} alone has been considered since work hardening is maximum at the surface (see Fig. 3

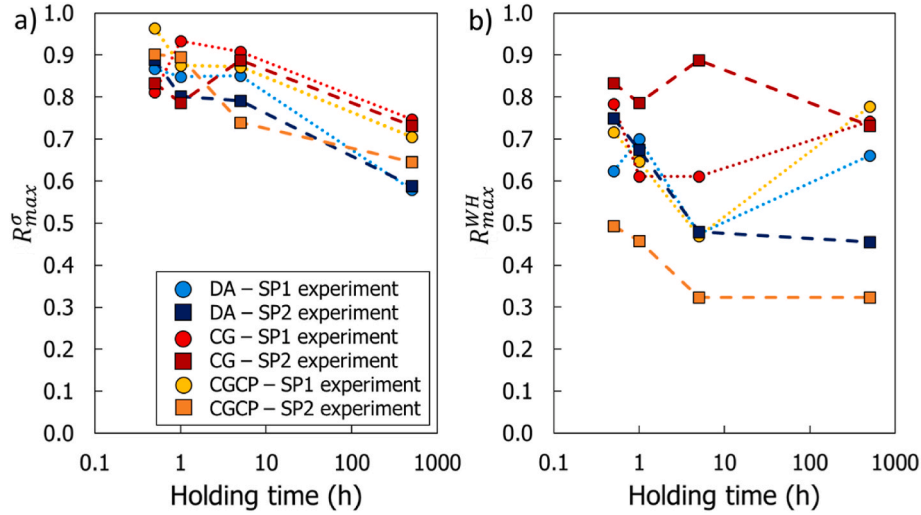


Fig. 10. Evolution of a) R_{max}^{σ} and b) R_{max}^{WH} as a function of holding time at 550 °C for the three microstructures and the two shot peening conditions.

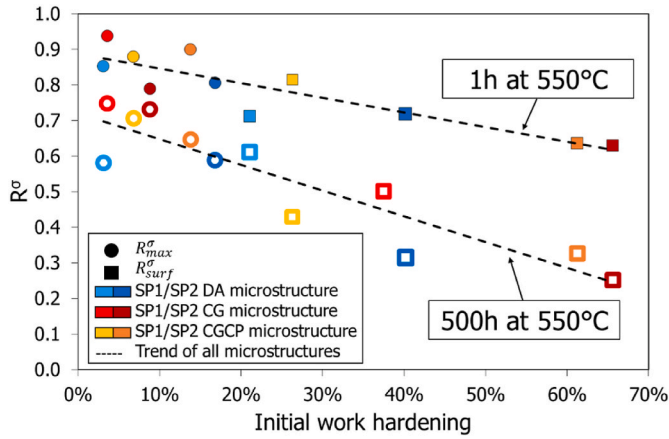


Fig. 11. Evolution of R^{σ} as a function of the initial work hardening value. R_{surf}^{σ} and R_{max}^{σ} values are indicated by circles and squares respectively. The definition of these parameters is given in Eq. (3). Only results for two holding times (1h and 500h) are presented.

Table 8

Value of R_{max}^{σ} after 500 h of holding time at 550 °C for the three microstructures and the two shot peening conditions.

	Direct Aged microstructure	Coarse grain microstructure	Coarse strengthening precipitates microstructure
SP1	0.59	0.75	0.71
SP2	0.59	0.73	0.65

for the definition of σ_{surf} , $z_{\sigma_{max}}$ and WH_{surf}). The following ratios as detailed in Section 2.3.2 can then be defined:

$$R_{surf}^{\sigma}(t_h) = \frac{\sigma(t_h, 0)}{\sigma_{ref}(0)} \quad R_{max}^{\sigma}(t_h) = \frac{\sigma(t_h, z_{\sigma_{max}})}{\sigma_{ref}(z_{\sigma_{max}})} \quad R_{max}^{WH}(t_h) = \frac{WH(t_h, 0)}{WH_{ref}(0)} \quad \text{Eq. 3}$$

The evolution of R_{surf}^{σ} as a function of holding time is shown in Fig. 9 for the DA microstructure and the two shot peening conditions. A significant evolution of the surface residual stresses occurs in the early stages (before 5 h); between 5 and 500 h, the surface residual stresses relax at a significantly lower rate. Very similar results were obtained for the other two microstructures and are thus not presented here.

The evolutions of R_{max}^{σ} and R_{max}^{WH} are shown in Fig. 10 as a function of holding time, for the three microstructures and the two shot peening

conditions; note that a logarithmic scale has been adopted for the holding time. As a whole, the results enable to identify some trends concerning the evolution of the different variables as a function of holding time (note the scale is logarithmic): (i) a significant evolution of the maximum residual stresses and work hardening occurs for holding times below 5 h; this was also observed for the surface residual stress; (ii) for holding times above 5 h, the relaxation of the residual stresses is reduced and the work hardening is slowed down, particularly for SP2. Comparing Figs. 9 and 10, it is also clear that R_{max}^{σ} is higher than R_{surf}^{σ} . For example, for the DA microstructure, SP2 shot peening condition, and after a holding time $t_h = 5$ h, $R_{max}^{\sigma} = 0.8$ while $R_{surf}^{\sigma} = 0.55$. This means that the relaxation of residual stresses is maximum at the surface. These results are related to the initial work hardening value introduced during shot peening. The higher the work hardening value, the higher the relaxation of the residual stresses. To visualize this, the values R_{surf}^{σ} and R_{max}^{σ} can be plotted as a function of the initial work hardening. Fig. 11 presents the results obtained for two holding times (1 h and 500 h). For a given holding time, a linear relationship is obtained between the normalized unrelaxed residual stress R^{σ} and the initial work hardening. The longer the holding time, the greater the influence of work hardening. It is interesting to note that the three microstructures follow a very similar trend. These results show work hardening is the dominant parameter in the relaxation of residual stresses. The influence of the microstructure on the relaxation of the residual stresses is only of second order.

3.3.4. Influence of the microstructure

If we want to identify the second order influence of the microstructure on the relaxation of residual stresses, it is necessary to remove the influence of work hardening. To do this, it is essential to analyze points with similar work hardening levels, or at least with sufficiently low work hardening levels, so that this parameter has the minimum impact on the analysis. It is interesting to notice that, for the depth $z_{\sigma_{max}}$, work hardening is five times lower than the surface work hardening (see for example Fig. 6). Moreover, it is relatively similar for the two shot peening conditions and the three microstructures (comparing Figs. 6–8). The influence of the microstructure can then be determined by observing the evolution of R_{max}^{σ} (Fig. 10a). A holding time of 500 h is chosen to analyze the results because the effects are more pronounced in this case. The results are shown in Table 8. An increase in grain size leads to a decrease in the thermal relaxation of residual stresses. The influence of a change in the size of the strengthening precipitates is more questionable. An increase in the size of the precipitates leads to a slight increase in the relaxation of residual stresses.

Table 9

Values of the coefficients identified for the different shot peening conditions and the different microstructures at two depths ($z_{\sigma_{surf}}$; $z_{\sigma_{max}}$).

Parameter	Depth	DA-SP1	DA-SP2	CG-SP1	CG-SP2	CGCP-SP1	CGCP-SP2
A	$z_{\sigma_{surf}}$	6.56E-02	1.91E-01	8.21E-02	2.05E-01	3.17E-01	1.43E-01
	$z_{\sigma_{max}}$	1.96E-01	1.88E-01	1.24E-01	6.82E-02	2.57E-01	2.11E-01
m	$z_{\sigma_{surf}}$	3.04E-07	5.59E-03	2.31E-05	6.84E-03	1.96E-03	3.03E-03
	$z_{\sigma_{max}}$	6.28E-05	8.11E-05	2.52E-08	9.89E-12	4.95E-05	7.40E-05

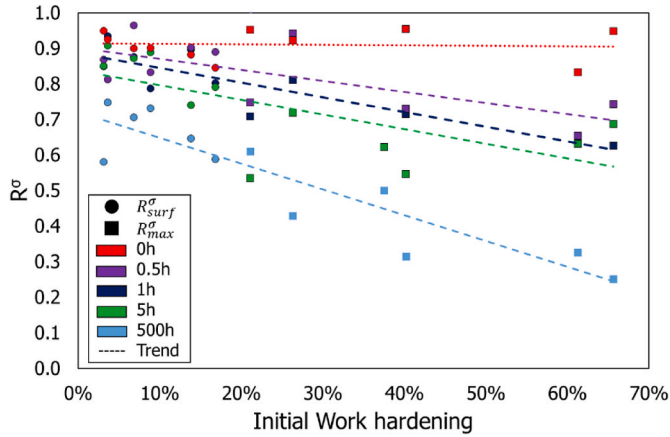


Fig. 12. Evolution of R^σ as a function of the initial work hardening level without distinction of microstructure and for different holding times and for the two depth locations $z_{\sigma_{surf}}$ and $z_{\sigma_{max}}$.

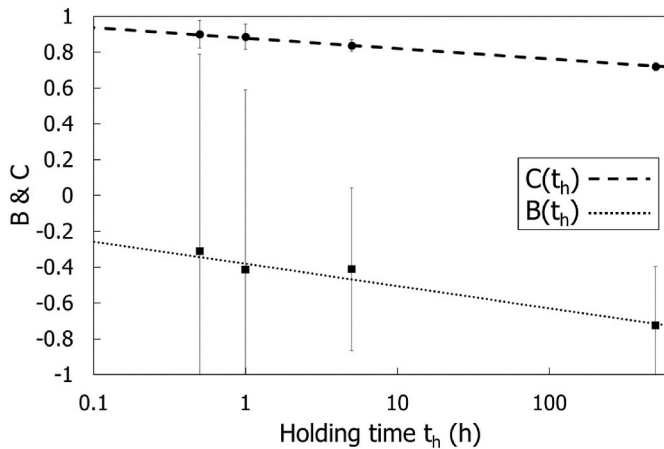


Fig. 13. Evolution of $B(t_h)$ and $C(t_h)$ as a function of holding time.

Table 10

Values of the parameters of the model of Eq. (9) for Inconel 718.

b_1	b_2	c_1	c_2
-0.130	-0.364	-0.061	0.907

Note that the parameters $B(t_h)$ and $C(t_h)$ could be modified to include a dependence on temperature. By considering different temperatures in an experimental campaign, an exponential form with temperature dependence could be considered for these parameters. This constitutes a perspective on the present work.

To explain this dependence on the microstructure, we consider the mobility of dislocations. Dislocations are the main vector of the plastic deformation introduced into the microstructure by shot peening. Because of the strong plastic strain introduced during the process, a rearrangement of the dislocations towards lower distortion energies occurs during the first moments at high temperature (Vöhringer and

NIKU-LARI, 1987). The more the dislocation structure is disturbed, the more it has to rearrange itself to reach an equilibrium level. This reorganization within the material leads to a relaxation of the residual stresses. The phenomena observed here are of the recovery process type. However, similarities can be drawn from studies dealing with the influence of microstructure on the creep behavior of Inconel 718. For a creep load, it has been shown in the literature that the influence of microstructural parameters in order of importance in Inconel 718 are: grain size, morphology and distribution of the δ phase and the size of the strengthening precipitates γ'/γ'' (Pieraggi and Uginet, 1994), (Chen and Chaturvedi, 1997), (Schafrik et al., 2001). As the grain size increases, the linear density of grain boundaries decreases, leading to a limitation of grain boundary slip and diffusion mechanisms at high temperatures. The δ phase appears to be the most important microstructural parameter on creep at an equivalent grain size. The lower the proportion of δ phase at the grain boundaries, the better the creep resistance. Moreover, a globular morphology is to be preferred to an acicular one to limit creep (Pieraggi and Uginet, 1994). Finally, the size of the strengthening precipitates γ'/γ'' can play a major role at fixed grain size and δ phase fraction, depending on the structural hardening mechanism involved. In the modified microstructures of this study, the transition from DA to CG microstructure mainly leads to an increase in grain size by a factor of 5 (see Table 5). Thus, the differences observed between the DA and CG microstructures are essentially related to the increase in grain size. Grain size, δ phase density, and distribution are similar between the two modified microstructures (CG and CGCP). The size of the strengthening precipitates is the only factor that causes a factor of ten difference between the two microstructures. According to Sundararaman, the size of the strengthening precipitates that causes a change in the precipitate shearing mechanisms is around 10 nm in the case of Inconel 718 (Sundararaman, 1988). In the present work, the size of the precipitates is greater than this value (20 and 200 nm see Table 6) for all the studied microstructures, so that a bypass type of Orowan mechanism occurs. When a dislocation bypasses an obstacle, it may create more dislocations. These newly formed dislocations are usually mobile and can move through the crystal lattice. This mechanism can thus increase the number of mobile dislocations in the material (Sundararaman, 1988). As a result, during holdings at 550 °C, the dislocations rearrange more easily as the size of the precipitates increases. This leads to an easier return to an equilibrium state and, thus, to a more significant relaxation of the residual stresses. However, since the impact of the size of the strengthening precipitates is of third order, the influence of a modification of their size on the relaxation of the residual stresses appears to be moderate in this work, and this despite a factor of 10 between the two modified microstructures.

4. A model for the thermal relaxation of residual stresses

The experimental results section confirms the previously obtained results in the literature (Masmoudi Khebou, 1990), (Lillamand, 1999), (Hoffmeister et al., 2008), (Prevéy et al., 1998). It also clearly demonstrates the influence of work hardening on residual stress relaxation. It is now proposed to build on these results to provide a model that allows the assessment of residual stress relaxation. The first proposal is to evaluate the existing Zener-Wert-Avrami model using these data. Then, a new model considering work hardening is proposed. The model's validation is conducted by comparing it with our experimental data and

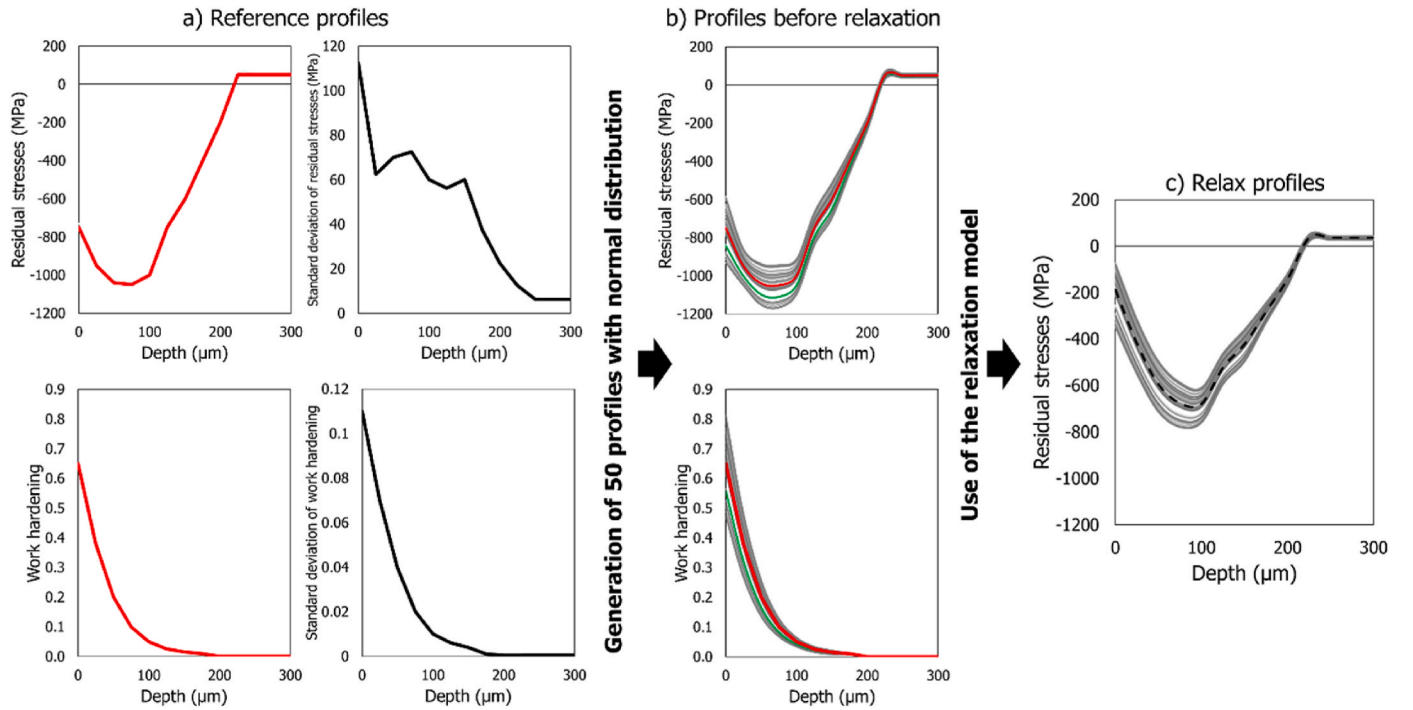


Fig. 14. Steps of the statistical procedure used to validate the model of residual stress relaxation. The red curve represents the reference profiles. The green curves represent an example of a pair of profiles generated with the normal distribution. (For interpretation of the references to color in this figure legend, the reader is referred to the Web version of this article.)

complementary results from the literature. Finally, an example is provided to demonstrate the model's application.

4.1. The Zener-Wert-Avrami model

The Zener-Wert-Avrami model is an empirical equation widely used in the literature to describe the evolution of a thermally activated process (Fine, 1964). It was first used by Vöhringer in 1987 to describe the relaxation of residual stresses (Vöhringer and NIKU-LARI, 1987). Since its introduction, this model has been used by many authors on different materials (steels, nickel-based alloys, titanium and aluminum alloys) (Hoffmeister et al., 2008), (Juijerm and Altenberger, 2006), (Vöhringer and NIKU-LARI, 1987), (Berger and Gregory, 1999), (Feng et al., 2009). This model allows for the determination of the stress relaxation $\sigma(T, t_h)$ at a given depth relative to the initial stress at the same depth σ_{ref} , as a function of the holding time t_h and the temperature T using the following equation:

$$\frac{\sigma(T, t_h)}{\sigma_{ref}} = \exp\left(-\left[C \exp\left(-\frac{\Delta H_A}{k T}\right) t_h\right]^m\right) \quad \text{Eq. 4}$$

where ΔH_A is the activation enthalpy, k is the Boltzmann constant, C and m are material parameters to be identified for each position in the component.

In this work, since the tests are all performed at the same temperature, Eq. (4) is reduced to:

$$\frac{\sigma(t_h)}{\sigma_{ref}} = \exp(-[A \cdot t_h]^m) \quad \text{Eq. 5}$$

A and m have then to be identified for each manufacturing process, each microstructure, and each point in the structure.

To evaluate the ability of the Zener-Wert-Avrami model to reproduce the experimental results of the present study, the parameters A and m have been identified for the experimental data presented Section 2; a least square method has been applied for each microstructure, for each shot peening condition and for each position, $z_{\sigma_{surf}^{RS}}$ and $z_{\sigma_{max}^{RS}}$. The

corresponding sets of values for A and m are presented in Table 9. Note that the parameters obtained, A and m , are simply the values that best fit the proposed empirical (Eq. (5)) for predicting residual stress relaxation. No physical meaning can be attached to these values. As expected, these values depend on the shot peening conditions and the microstructure. Note that the m parameter is the most affected by the position and thus by work hardening. The Zener-Wert-Avrami model is mainly devoted to the prediction of relaxation as a function of the temperature. Due to the substantial impact of work hardening on the thermal relaxation of residual stresses, and the large range of hardening in the structure induced by shot peening, this model is not suitable for the description of the thermal relaxation of a complete residual stress profile or others shot peening conditions.

4.2. A model for thermal residual stress relaxation accounting for work hardening

A model, which considers the work hardening state and considers holding time and position, is proposed to predict the relaxation of residual stresses. This model is based on the experimental observations presented in Section 2. The aim of the model is to be independent of the manufacturing process that generated the residual stresses. In addition, its relative simplicity (analytical) is crucial to function as a practical tool for validating the conditions of a prestressing manufacturing process and its parameters in an industrial context. It has been shown that the microstructural impact on the thermal relaxation of residual stresses is small compared to that of work hardening (see Section 2.3). It is thus decided to disregard the influence of the microstructure to define the model. We then study the residual stress ratio R^σ (defined Eq. (3)) at two specific locations $z_{\sigma_{surf}}$ and $z_{\sigma_{max}}$ as a function of the initial work hardening level. These results are presented in Fig. 12 for all the investigated holding times; note that in this figure, the microstructure has not been identified to simplify the reading since we disregard its influence. Shot peening conditions are considered on the basis of the level of work hardening they cause. Therefore, in the same way, they are not explicitly shown in Fig. 12. A linear regression has been conducted for the data

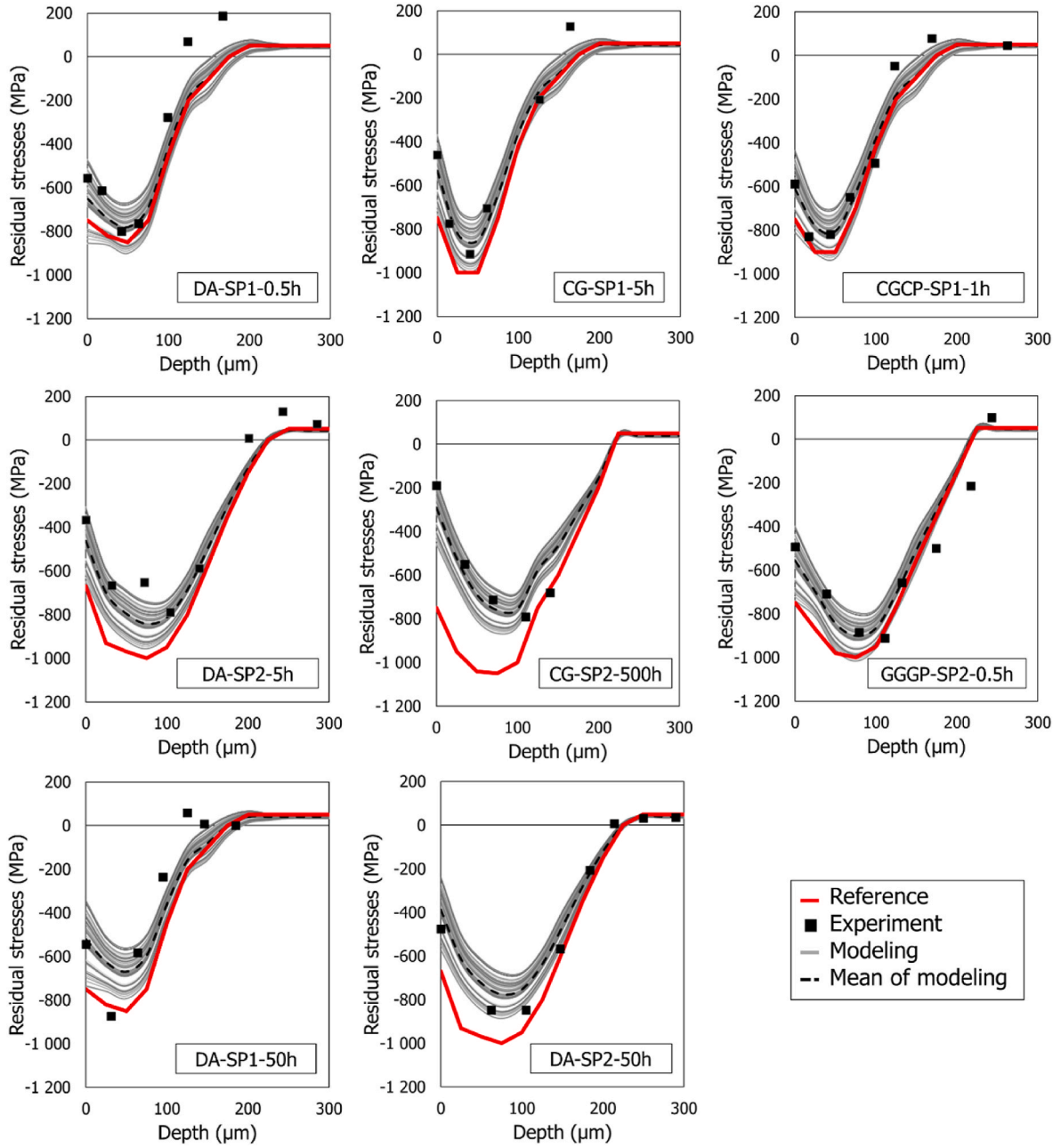


Fig. 15. Comparison between experimental data and modeling. The labels in the graphs indicate: the microstructure – the shot peening condition – the holding time.

points corresponding to each specified holding time. Comparing the experimental results and the straight line obtained with the linear regression, we make the hypothesis that, for a given holding time, the ratio of unrelaxed residual stresses depends linearly on the initial value of the work hardening and can be expressed as follows:

$$R^\sigma(t_h, z) = B(t_h) \cdot WH(z) + C(t_h) \tag{Eq. 6}$$

where $WH(z)$ is the initial work hardening value at the depth z (with a range between 0 and 1) and, $B(t_h)$ and $C(t_h)$ are functions that depend on the holding time.

The parameters B and C are evaluated for each straight line in Fig. 12 and for each holding time; the corresponding results are shown in Fig. 13. These two parameters exhibit a rapid evolution for the shorter holding times, followed by a stabilization for the longest holding time. It is therefore proposed to describe the evolution of $C(t_h)$ and $B(t_h)$ with a logarithmic function such that:

$$B(t_h) = b_1 \log_{10}(t_h) + b_2 \tag{Eq. 7}$$

$$C(t_h) = c_1 \log_{10}(t_h) + c_2 \tag{Eq. 8}$$

with b_1, b_2, c_1 and c_2 being constant parameters that need to be identified. Considering this formulation, for $t_h = 0$, the model gives $B(0) \neq 0$ and $C(0) \neq 1$. Therefore, the model may appear erroneous for holding times less than 0.029 h (i.e., 2 min). However, given the holding times used in the proposed applications (greater than 30 min), and in the interest of model simplicity, this model is considered in the following, as is Eq. (6). Other formulation using exponential function could be used to respect that the residual stress profile being then the initial one as expected ($B(0) = 0$ and $C(0) = 1$).

Also note that in the model a residual stress relaxation can be obtained even if there is no work hardening ($WH(0) = 0$) in the material. Finally, the proposed model that estimates the ratio of unrelaxed re-

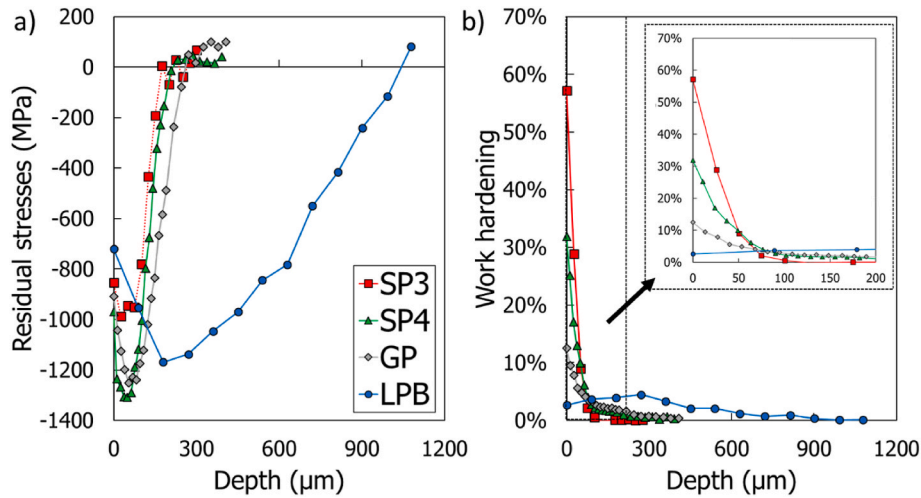


Fig. 16. Residual stresses (a) and work hardening (b) profiles produced by shot peening (SP3 and SP4), gravity peening, and low plastic Burnishing in IN718 (Prevéy, 2000).

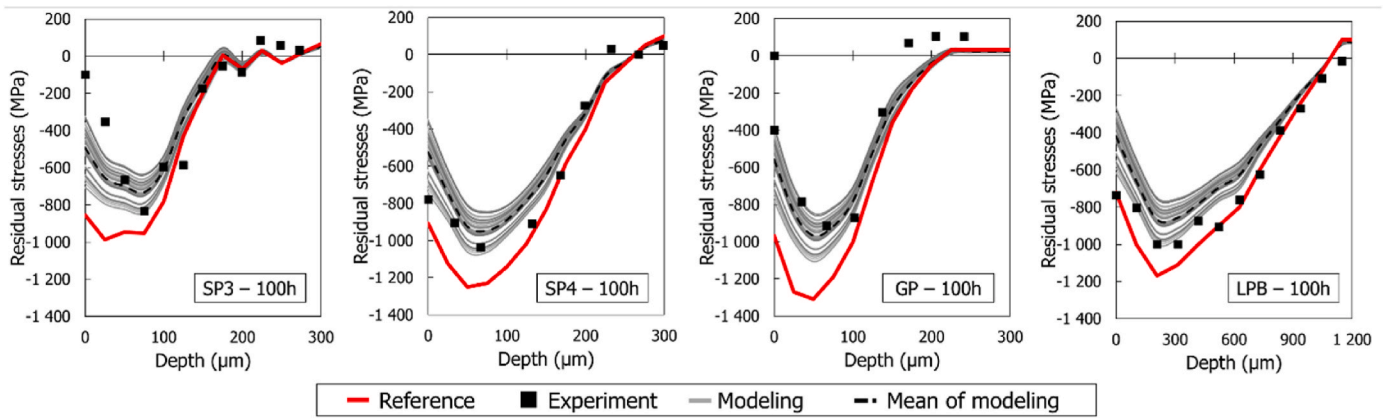


Fig. 17. Comparison between experiment (Prevéy, 2000) and modeling of residual stress profiles after 100h holding time at 525 °C.

Residual stresses takes the form:

$$R^\sigma(t_h, z) = [b_1 \log_{10}(t_h) + b_2] \cdot WH(z) + c_1 \log_{10}(t_h) + c_2 \quad \text{Eq. 9}$$

The four material parameters b_1 , b_2 , c_1 and c_2 have been identified for Inconel 718 with a least square method on the data presented in Fig. 13. The obtained values are given in Table 10. Note that given the model form in Eq. (9), only three holding time values are sufficient to identify the model, such as the initial residual stress and work hardening levels and the residual stress and work hardening levels after 5 h and 500 h of holding time.

4.3. Model validation

The model proposed in the previous section is now employed to predict the relaxation of residual stresses under varying conditions. These conditions differ from those of the previous analysis used to identify the parameters. Three sets of experimental data are considered:

- i) The part of the results presented in Section 2.3 that have not been used to identify the parameters, that is for positions other than $z_{\sigma_{surf}}$ and $z_{\sigma_{max}}$.
- ii) Additional measurements that have been performed in the framework of the present study for the DA microstructure and for 50 h of holding time at 550 °C following the protocol detailed Section 1.3.

- iii) Data from Prévéy's work (Prevéy, 2000) which allows the model to be validated under experimental conditions not investigated here.

For all these data, a statistical analysis has been carried out to consider the experimental scatter and the possible errors in the identification of the model. The different steps of this statistical procedure are illustrated in Fig. 14. With this objective, a pair of initial residual stress and work hardening profiles (solid red lines) have been used as the average values of the normal distribution (Fig. 14a). The standard deviation considered in the normal distribution is characteristic of the observed experimental scatter. Fifty pairs of initial residual stress and work hardening profiles have been generated following this procedure (examples of such profiles are shown in green in Fig. 14b). Then, the model presented in Section 3.2 is applied to all these pairs of profiles to obtain 50 profiles of relaxed residual stresses (solid grey lines in Fig. 14c). The average of these profiles is then computed (dashed black line).

This procedure has been first applied to the experimental data obtained in the campaign carried out in this work. The results are presented in Fig. 15. For all shot peening conditions and microstructures considered, the average values predicted by the model are in accordance with the experimental data. It is worth noting that the model reproduces particularly well the surface relaxation of the residual stress level, which

is strongly influenced by the high level of work hardening. The methodology implemented permits estimation of the relaxation of the residual stresses for the whole depth affected by the process. Additionally, by incorporating experimental dispersion into the procedure, significant variations in residual stress profiles within similar surface treatment and heat treatment conditions can be accurately reflected. These results are consistent with the experimental observations.

The statistical procedure has also been applied to experimental data obtained by Prev y for Inconel 718 (Prev y, 2000). In Prev y's work, the residual stress and work hardening profiles have been evaluated for different surface treatments before and after a heat treatment at 525 °C for 100 h; two shot peening conditions (here denoted *SP3* and *SP4*) as well as gravity peening (here noted *GP*) and low plastic burnishing (here noted *LPB*) treatments have been studied. Fig. 16 presents the initial residual stress and work hardening profiles extracted from (Prev y, 2000) for the different processes. Note that these four surface treatments provide a variety of residual stress and work hardening profiles. The test conditions differ from those of our study (material, measurement conditions, heat treatment temperature); the microstructure is not given. These results thus constitute an interesting test for the model proposed in Section 3.2. Fig. 17 depicts the residual stress relaxation profiles obtained through experimentation (Prev y, 2000) and the profiles predicted by the model using the statistical analysis outlined above. Once again, the model successfully replicates the trends of the experimental results obtained by Prev y. Notably, the model accurately estimates the maximum level of residual stress after 100h of holding time at 525 °C. The relaxation of surface residual stresses could be more accurate, as in the previous example in Fig. 15. However, this analysis confirms the relevance and the pertinence of the proposed modeling.

5. Conclusion

The aim of this work was to establish a model for the influence of work hardening and microstructure on the evolution of residual stresses under thermal loading. The first step was to analyze the numerous experimental conditions used in this study to assess the effect of work hardening, grain size and size of strengthening precipitates on the relaxation of residual stresses. Residual stress and work hardening profiles were determined on shot peened components for different holding times at 550 °C. The calibration methodology previously proposed (Goulmy et al., 2021a) allows the influence of different microstructures in terms of grain size and precipitate size to be evaluated. It has been possible to establish the order of influence of the parameters on the relaxation of residual stresses under thermal loading. The first order parameter is work hardening. The higher it is, the greater the relaxation of residual stresses. The second order parameter is grain size. An increase in this factor leads to a decrease in residual stress relaxation. Finally, the parameter with the least influence in the study carried out was the size of the strengthening precipitates, where no clear trend could be deduced from the experimental data analyzed.

Based on the experimental results, an analytical model was then proposed which considers the influence of the work hardening induced by the surface treatment. Several advantages of this model can be highlighted. The parameters of the model can be identified on the basis of characteristic points present on the residual stress profiles; at the surface and where the compressive residual stresses are at their maximum. As a result, only a few points are required to calibrate the model. Once identified, it can be used to predict the relaxation of residual stresses in depth if the work hardening profile induced by the surface treatment is known. The proposed model is not limited to the case of shot peening. It can now be applied to estimate the relaxation of residual stresses on components that may have a work hardening gradient in the part. As explained in the introduction, shot-peened Inconel 718 parts are subject to temperature fatigue loading. The study carried out here will therefore make it possible to decouple the effects of mechanical loading and temperature.

CRedit authorship contribution statement

J.P. Goulmy: Writing – original draft, Investigation. **L. Toualbi:** Writing – original draft, Supervision, Investigation. **V. Boyer:** Investigation. **P. Kanoute:** Writing – review & editing, Supervision, Conceptualization. **D. Retraint:** Writing – review & editing, Supervision, Conceptualization. **E. Rouhaud:** Writing – review & editing, Supervision, Conceptualization.

Declaration of competing interest

The authors declare that they have no known competing financial interests or personal relationships that could have appeared to influence the work reported in this paper.

Data availability

Data will be made available on request.

Acknowledgement

This work was conducted with the help of the French Technological Research Institute for Materials, Metallurgy and Processes (IRT M2P) under the CONDOR project. The authors would like to acknowledge IRT M2P and all the partners of the project led by IRT M2P. Safran is warmly thanked for its precious collaboration in this work.

References

- Alexandre, F., Deyber, S., Pineau, A., 2004. Modelling the optimum grain size on the low cycle fatigue life of a Ni based superalloy in the presence of two possible crack initiation sites. *Scripta Mater.* 50 (1), 25–30. <https://doi.org/10.1016/j.scriptamat.2003.09.043>.
- Atig, A., Ben Sghaier, R., Seddik, R., Fathallah, R., 2018. Probabilistic methodology for predicting the dispersion of residual stresses and Almen intensity considering shot peening process uncertainties. *Int. J. Adv. Manuf. Technol.* 94 (5), 2125–2136. <https://doi.org/10.1007/s00170-017-1033-3>.
- Benedetti, M., Fontanari, V., Santus, C., Bandini, M., 2010. Notch fatigue behaviour of shot peened high-strength aluminium alloys: experiments and predictions using a critical distance method. *Int. J. Fatig.* 32 (10), 1600–1611. <https://doi.org/10.1016/j.ijfatigue.2010.02.012>.
- Berger, M.-C., Gregory, J.K., 1999. Residual stress relaxation in shot peened Timetal 21s. *Mater. Sci. Eng., A* 263 (2), 200–204. [https://doi.org/10.1016/S0921-5093\(98\)01165-4](https://doi.org/10.1016/S0921-5093(98)01165-4).
- Bhuiyan, M.D., Mutoh, Y., McEvily, A.J., 2012. The influence of mechanical surface treatments on fatigue behavior of extruded AZ61 magnesium alloy. *Mater. Sci. Eng., A* 549, 69–75. <https://doi.org/10.1016/j.msea.2012.04.007>.
- Cai, D., Nie, P., Shan, J., Liu, W., Gao, Y., Yao, M., 2006. Precipitation and residual stress relaxation kinetics in shot-peened Inconel 718. *J. Mater. Eng. Perform.* 15 (5), 614–617. <https://doi.org/10.1361/105994906X124613>.
- Cammett, J.T., Prev y, P.S., Jayaraman, N., 2005. The effect of shot peening coverage on residual stress, cold work, and fatigue in a Nickel-Base Superalloy. In: *ICSP 9, Paris*.
- Chen, W., Chaturvedi, M.C., 1997. Dependence of creep fracture of Inconel 718 on grain boundary precipitates. *Acta Mater.* 45 (7), 2735–2746. [https://doi.org/10.1016/S1359-6454\(96\)00399-0](https://doi.org/10.1016/S1359-6454(96)00399-0).
- Daoud, M., Kubler, R., Bemou, A., Osmond, P., Polette, A., 2021. Prediction of residual stress fields after shot-peening of TRIP780 steel with second-order and artificial neural network models based on multi-impact finite element simulations. *J. Manuf. Process.* 72, 529–543. <https://doi.org/10.1016/j.jmpro.2021.10.034>.
- Fathallah, R., Inglebert, G., Castex, L., 1998. Prediction of plastic deformation and residual stresses induced in metallic parts by shot peening. *Mater. Sci. Technol.* 14 (7), 631–639. <https://doi.org/10.1179/mst.1998.14.7.631>.
- Feng, B.X., Mao, X.N., Yang, G.J., Yu, L.L., Wu, X.D., 2009. Residual stress field and thermal relaxation behavior of shot-peened TC4-DT titanium alloy. *Mater. Sci. Eng., A* 512 (1–2), 105–108. <https://doi.org/10.1016/j.msea.2009.01.028>.
- Fine, M.E., 1964. *Introduction To Phase Transformations In Condensed Systems*, First Printing. Macmillan, New York [Online]. Available: <https://www.biblio.com/book/introduction-phase-transformations-condensed-systems-fine/d/1298436554>. (Accessed 19 April 2024).
- Foss, B.J., Gray, S., Hardy, M.C., Stekovic, S., McPhail, D.S., Shollock, B.A., 2013. Analysis of shot-peening and residual stress relaxation in the nickel-based superalloy RR1000. *Acta Mater.* 61, 2548–2559.
- Gerin, B., Pessard, E., Morel, F., Verdu, C., 2017. Influence of surface integrity on the fatigue behaviour of a hot-forged and shot-peened C70 steel component. *Mater. Sci. Eng., A* 686, 121–133. <https://doi.org/10.1016/j.msea.2017.01.041>.

- Goulmy, J.P., et al., 2021a. A calibration procedure for the assessment of work hardening part I: effects of the microstructure and load type. *Mater. Char.* 175, 111067 <https://doi.org/10.1016/j.matchar.2021.111067>.
- Goulmy, J.P., et al., 2021b. A calibration procedure for the assessment of work hardening Part II: application to shot peened IN718 parts. *Mater. Char.* 175, 111068 <https://doi.org/10.1016/j.matchar.2021.111068>.
- Goulmy, J.P., Boyer, V., Retraint, D., Kanoute, P., Toualbi, L., Rouhaud, E., 2023. Modeling of the shot peening of a nickel alloy with the consideration of both residual stresses and work hardening. *Int. J. Solid Struct.* 264, 112120 <https://doi.org/10.1016/j.ijsolstr.2023.112120>.
- Hoffmeister, J., Schulze, V., Wanner, A., Hessert, R., Koenig, G., 2008. Thermal relaxation of residual stresses induced by shot peening in IN718. In: *10th International Conference Of Shot Peening*, Tokyo [Online]. Available: <http://www.shopteener.com/library/pdf/2008060.pdf>. (Accessed 12 March 2015).
- Hoffmeister, J., Schulze, V., Hessert, R., Koenig, G., 2011. Effects of the surface treatment on the measured diffraction peak width of Inconel 718. In: ICSP-11, pp. 201–206 [Online]. Available: <http://www.shopteener.com/library/pdf/2011033.pdf>. (Accessed 11 April 2017).
- Juijerm, P., Altenberger, I., 2006. Residual stress relaxation of deep-rolled Al–Mg–Si–Cu alloy during cyclic loading at elevated temperatures. *Scripta Mater.* 55 (12), 1111–1114. <https://doi.org/10.1016/j.scriptamat.2006.08.047>.
- Kamaya, M., Wilkinson, A.J., Titchmarsh, J.M., 2004. Measurement of plastic strain of polycrystalline material by electron backscatter diffraction. *Nucl. Eng. Des.* 235, 713–725.
- Klotz, T., Delbergue, D., Bocher, P., Lévesque, M., Brochu, M., 2018. Surface characteristics and fatigue behavior of shot peened Inconel 718. *Int. J. Fatig.* 110, 10–21. <https://doi.org/10.1016/j.ijfatigue.2018.01.005>.
- Lillamand, I., 1999. Evolution d'une couche grenillée sous sollicitations thermiques et mécaniques, cas de la fatigue oligocyclique. Thèse de doctorat, ENSAM.
- Lu, J., 1996. Handbook of Measurement of Residual Stresses. Fairmont Press, Lilburn, GA, Upper Saddle River, NJ. Distributed by Prentice Hall PTR.
- Masmoudi Khebou, N., 1990. Etude de l'évolution des contraintes de grenailage en fatigue à haute température pour le superalliage base nickel IN100. Thèse Doctorat, Arts et Métiers ParisTech. France.
- Norme AFNOR NFL 06-832, 1990.
- Pieraggi, B., Uginet, J.F., 1994. Fatigue and creep properties in relation with alloy 718 microstructure. In: *Superalloys 718, 625, 706 and Various Derivatives*. TMS, pp. 535–544. https://doi.org/10.7449/1994/Superalloys_1994_535_544, 1994.
- Prevéy, P.S., 1987. The measurement of sub-surface residual stress and cold work distributions in nickel base alloys. In: *Residual Stress in Design, Process and Materials Selection*, pp. 11–19.
- Prevéy, P.S., 2000. The effect of cold work on the thermal stability of residual compression in surface enhanced IN718. In: *20th ASM Materials Solutions Conference & Exposition*, St. Louis, Missouri.
- Prevéy, P.S., Hornbach, D.J., Mason, P.W., 1998. Thermal Residual Stress Relaxation and Distortion in Surface Enhanced GasTurbine Engine Components. *ASM International*.
- Qin, Z., Li, B., Zhang, H., Youani Andre Wilfried, T., Gao, T., Xue, H., 2022. Effects of shot peening with different coverage on surface integrity and fatigue crack growth properties of 7B50-T7751 aluminum alloy. *Eng. Fail. Anal.* 133, 106010 <https://doi.org/10.1016/j.engfailanal.2021.106010>.
- Schafrik, R.E., Ward, D.D., Groh, J.R., 2001. Application of alloy 718 in GE aircraft engines: past, present and next five years. In: *Superalloys 718, 625, 706 and Various Derivatives*. TMS, pp. 1–11. https://doi.org/10.7449/2001/Superalloys_2001_1_11, 2001.
- Schulze, V., Burgahn, F., Vöhringer, O., Macherauch, E., 1993. Zum thermischen Abbau von Kugelstrahl-Eigenstressungen bei vergütetem 42 CrMo 4. *Mat.-wiss. u. Werkstofftech.* 24 (7), 258–267. <https://doi.org/10.1002/mawe.19930240709>.
- Soady, K.A., Mellor, B.G., West, G.D., Harrison, G., Morris, A., Reed, P.A.S., 2013. Evaluating surface deformation and near surface strain hardening resulting from shot peening a tempered martensitic steel and application to low cycle fatigue. *Int. J. Fatig.* 54, 106–117. <https://doi.org/10.1016/j.ijfatigue.2013.03.019>.
- Sundaraman, P.M.M., 1988. Precipitation of the δ -Ni 3 Nb phase in two nickel base superalloys. *Metallurgical and Materials Transactions A-physical Metallurgy and Materials Science - METALL MATER TRANS A* 19 (3), 453–465. <https://doi.org/10.1007/BF02649259>.
- Surface Integrity, 1989. Tech report. Manufacturing Engineering.
- Vöhringer, O., 1987. Relaxation of residual stresses by annealing or mechanical treatment. In: NIKU-LARI, A. (Ed.), *Residual Stresses*. Pergamon, pp. 367–396 [Online]. Available: <http://www.sciencedirect.com/science/article/pii/B9780080340623500276>. (Accessed 23 March 2015).
- Zhou, Z., et al., 2011. A finite element study of thermal relaxation of residual stress in laser shock peened IN718 superalloy. *Int. J. Impact Eng.* 38 (7), 590–596. <https://doi.org/10.1016/j.ijimpeng.2011.02.006>.